Single Breath-Hold 3-Dimensional Magnetic Resonance Elastography Depicts Liver Fibrosis and Inflammation in Obese Patients

Omar Isam Darwish, Ahmed Gharib, Sami Jeljeli, Nader Metwalli, Jenna Feeley, Yaron Rotman, Rebecca Brown, Ronald Ouwerkerk, David Kleiner, Daniel Stäb, et al.

Single Breath-Hold 3-Dimensional Magnetic Resonance Elastography Depicts Liver Fibrosis and Inflammation in Obese Patients

Omar Isam Darwish, MPhil,†‡ Ahmed M. Gharib, MD,§ Sami Jeljeli, PG DIP,* Nader S. Metwalli, PhD,§ Jenna Feeley, BS,§ Yaron Rotman, MD, MSc,§ Rebecca J. Brown, MD, MHSc,§ Ronald Ouwerkerk, PhD,§ David E. Kleiner, MD, PhD,|| Daniel Stäb, PhD,¶ Peter Speier, PhD,# Ralph Sinkus, PhD,*† and Radhouene Neji, PhD*‡*

Objectives: Three-dimensional (3D) magnetic resonance elastography (MRE) measures liver fibrosis and inflammation but requires several breath-holds that hamper clinical acceptance. The aim of this study was to evaluate the technical and clinical feasibility of a single breath-hold 3D MRE sequence as a means of measuring liver fibrosis and inflammation in obese patients.

Methods: From November 2020 to December 2021, subjects were prospectively enrolled and divided into 2 groups. Group 1 included healthy volunteers (n = 10) who served as controls to compare the single breath-hold 3D MRE sequence with a multiple–breath-hold 3D MRE sequence. Group 2 included liver patients (n = 10) who served as participants to evaluate the clinical feasibility of the single breath-hold 3D MRE sequence in measuring liver fibrosis and inflammation. Controls and participants were scanned at 60 Hz mechanical excitation with the single breath-hold 3D MRE sequence to retrieve the magnitude of the complex-valued shear modulus (|G*| [kPa]), the shear wave speed (Cs [m/s]), and the loss modulus (G" [kPa]). The controls were also scanned with a multiple–breath-hold 3D MRE sequence for comparison, and the participants had histopathology (Ishak scores) for correlation with Cs and G".

Results: For the 10 controls, 5 were female, and the mean age and body mass index were 33.1 ± 9.5 years and 23.0 ± 2.1 kg/m^2, respectively. For the 10 participants, 8 were female, and the mean age and body mass index were 45.1 ± 16.5 years and 33.1 ± 4.0 kg/m^2 (obese range), respectively. All participants were suspected of having nonalcoholic fatty liver disease. Bland-Altman analysis of the comparison in controls shows there are nonsignificant differences in |G*|, Cs, and G" below 6.5%, suggesting good consensus between the 2 sequences. For the participants, Cs and G" correlated significantly with Ishak fibrosis and inflammation grades, respectively ($\rho = 0.95$, $P < 0.001$, and $\rho = 0.84$, $P = 0.002$).

Conclusion: The single breath-hold 3D MRE sequence may be effective in measuring liver fibrosis and inflammation in obese patients.

Key Words: 3-dimensional magnetic resonance elastography, single breath-hold, simultaneous multislice, liver, fibrosis, inflammation, nonalcoholic fatty liver disease, shear wave speed, loss modulus

(*Invest Radiol* 2023;58: 413–419)

Hepatic 2-dimensional (2D) magnetic resonance elastography (MRE) is widely used in quantifying liver fibrosis for its noninvasiveness. Two-dimensional MRE measures the magnitude of the complex shear modulus (|G*| [kPa]) that increases with liver fibrosis.[1] By comparison, hepatic 3D MRE has demonstrated promises using viscoelastic parameters derived from the 3D displacement field to quantify liver fibrosis and inflammation simultaneously.[2–4] 3D MRE allows for measuring the shear wave speed (Cs [m/s]) for fibrosis and the loss modulus (G" [kPa]) for inflammation.[2]

However, current 3D MRE sequences usually necessitate 4 to 6 multiple consecutive breath-holds.[3,5,6] Various approaches have been proposed to reduce the total acquisition time, including fractional motion encoding,[7] more flexible timing concepts,[5,6,8] and simultaneous multislice (SMS) excitation.[9] Despite the achieved acceleration for each method, they all still require multiple breath-holds, which hampers clinical acceptance and reduces the precision of the viscoelastic parameters owing to imperfect geometric alignment of the different breath-holds, especially in obese patients. Thus, a pivotal aspect to successfully deploying hepatic 3D MRE within the clinic is to reduce acquisition time, preferably to 1 single breath-hold that can be easily tolerated and reproduced by obese patients.

The present study aims to demonstrate the technical development and feasibility of a single breath-hold 3D MRE sequence that covers multiple slices, wave offsets, and motion encodings. Another purpose is to evaluate the clinical utility of this single breath-hold 3D MRE sequence in obese patients with nonalcoholic fatty liver disease (NAFLD) to quantify liver fibrosis and inflammation simultaneously. Patients with NAFLD are challenging owing to high body mass index (BMI) precluding adequate penetration of the mechanical waves and the expected magnetic resonance (MR) signal drop in the liver due to fat infiltration. In addition, NAFLD is a health crisis across the globe, and evaluating NAFLD in a time-efficient fashion is becoming of high importance in medicine.[10]

MATERIALS AND METHODS

Study Subjects

This prospective study was conducted from November 2020 to December 2021 and was approved by the local institutional review board.

Received for publication November 4, 2022; and accepted for publication, after revision, December 12, 2022.

From the *School of Biomedical Engineering and Imaging Sciences, King's College London, London, United Kingdom; †INSERM U1148, LVTS, University Paris Diderot, Paris, France; ‡MR Research Collaborations, Siemens Healthcare Limited, Frimley, United Kingdom; §National Institute of Diabetes and Digestive and Kidney Diseases, Bethesda, MD; ||National Cancer Institute, Bethesda, MD; ¶MR Research Collaborations, Siemens Healthcare Limited, Melbourne, Australia; and #MR Application Predevelopment, Siemens Healthcare GmbH, Erlangen, Germany.

Conflicts of interest and sources of funding: Omar Darwish is a PhD candidate, and their university tuitions fees are covered by Siemens Healthineers. Dr Radhouene Neji is an employee of Siemens Healthineers United Kingdom, Dr Daniel Stäb is an employee of Siemens Healthcare Australia, and Dr Peter Speier is an employee of Siemens Healthcare Germany. For the remaining authors, none were declared. Sources of funding: CRUK City of London Centre Award (C7893/A26233), CRUK (EDDCPGM/100001), Siemens Healthineers, ITMO Aviesan 2020 (DESP/PB n°241), National Institutes of Health intramural fund, and by US Agency for International Development (USAID) and National Academy of Sciences through Subaward 2000012771 (any opinions, findings, conclusions, or recommendations expressed are those of the authors alone, and do not necessarily reflect the views of USAID or National Academy of Sciences).

Correspondence to: Ahmed M. Gharib, MD, National Institutes of Health, Building 10, Room 1C334, Bethesda, MD 20892. E-mail: ahmed.gharib@nih.gov.

Supplemental digital contents are available for this article. Direct URL citations appear in the printed text and are provided in the HTML and PDF versions of this article on the journal's Web site (www.investigativeradiology.com).

ISSN: 0020-9996/23/5806–0413
DOI: 10.1097/RLI.0000000000000952

Two groups of subjects were enrolled after signing informed consent. Enrollees in group 1 (technical feasibility group) were healthy volunteers (n = 10) who served as controls to compare the single breath-hold 3D MRE sequence with a multiple–breath-hold 3D MRE sequence[5] and to validate the repeatability of the single breath-hold 3D MRE sequence. Individuals in group 2 (clinical feasibility group) were patients with NAFLD (n = 10). Stages and grades of liver fibrosis and inflammation of group 2 were assigned using Ishak scoring,[11] with a maximum fibrosis stage and inflammation grade of 6 and 18, respectively. In addition, hepatic fat fractions of group 2 were measured using a T2 corrected multiecho STEAM-based MR spectroscopy sequence termed HISTO.[12]

MRE Acquisition and Processing

Controls were scanned on a 3 T system (Biograph mMR, Siemens Healthcare, Erlangen, Germany) with a 6-channel body coil and a 24-channel spine coil, and participants were scanned on a 1.5 T system (MAGNETOM Aera, Siemens Healthcare) with an 18-channel body coil and a 32-channel spine coil. Both controls and participants were scanned in supine position.

MRE Acquisition

Both groups were scanned at 60 Hz mechanical excitation using the gravitational transducer[13] with the single breath-hold 3D MRE sequence. The gravitational transducer generates the mechanical excitation using a rotational eccentric mass placed on the abdomen of the subject driven by a 4-Nm stepper motor placed outside of the MR examination room through a 6-m flexible plastic rotating axis. The set-up time for the positioning of the gravitational transducer per subject was approximately 10 minutes. In addition, identical gravitational transducers were used at 1.5 and 3 T. The single breath-hold 3D MRE sequence concatenates 4 different motion encoding measurements, required to encode the 3D displacement field, and 4 mechanical wave offsets of 8 slices in 1 single breath-hold. The single breath-hold is achieved by these 3 following steps: (1) optimizing a previously developed multishot spoiled gradient echo (GRE) MRE sequence[6] that utilizes 2 integer parameters (N_d, N_w) to allow for an acquisition that is phase-locked to the mechanical vibration. N_w is an integer multiple of the mechanical wave period where all imaging shots for the same mechanical wave offset, k-space phase encoding line, and motion encoding measurement are acquired. N_d is an integer factor that extends the sequence delay to enable the acquisition of interleaved mechanical wave offsets. Here, we set N_d to 1 and optimized N_w to its smallest possible value (see Text, Supplemental Digital Content, http://links.lww.com/RLI/A799, which explains calculating optimal N_w) given a certain shot duration imposed by the chosen echo time (Figs. 1A–C). (2) Utilizing an in-plane generalized autocalibrating partially parallel acquisition (GRAPPA)–based SMS formulation[15] that provides a simple separation of the simultaneously excited slices N_{SMS} by oversampling the field of view (FOV) in the phase-encoding direction by a factor N_{SMS} and shifting the simultaneously excited slices in the oversampling region. The use of phase oversampling results in a nonaccelerated acquisition; however, the single breath-hold 3D MRE sequence acceleration is realized through the total in-plane GRAPPA

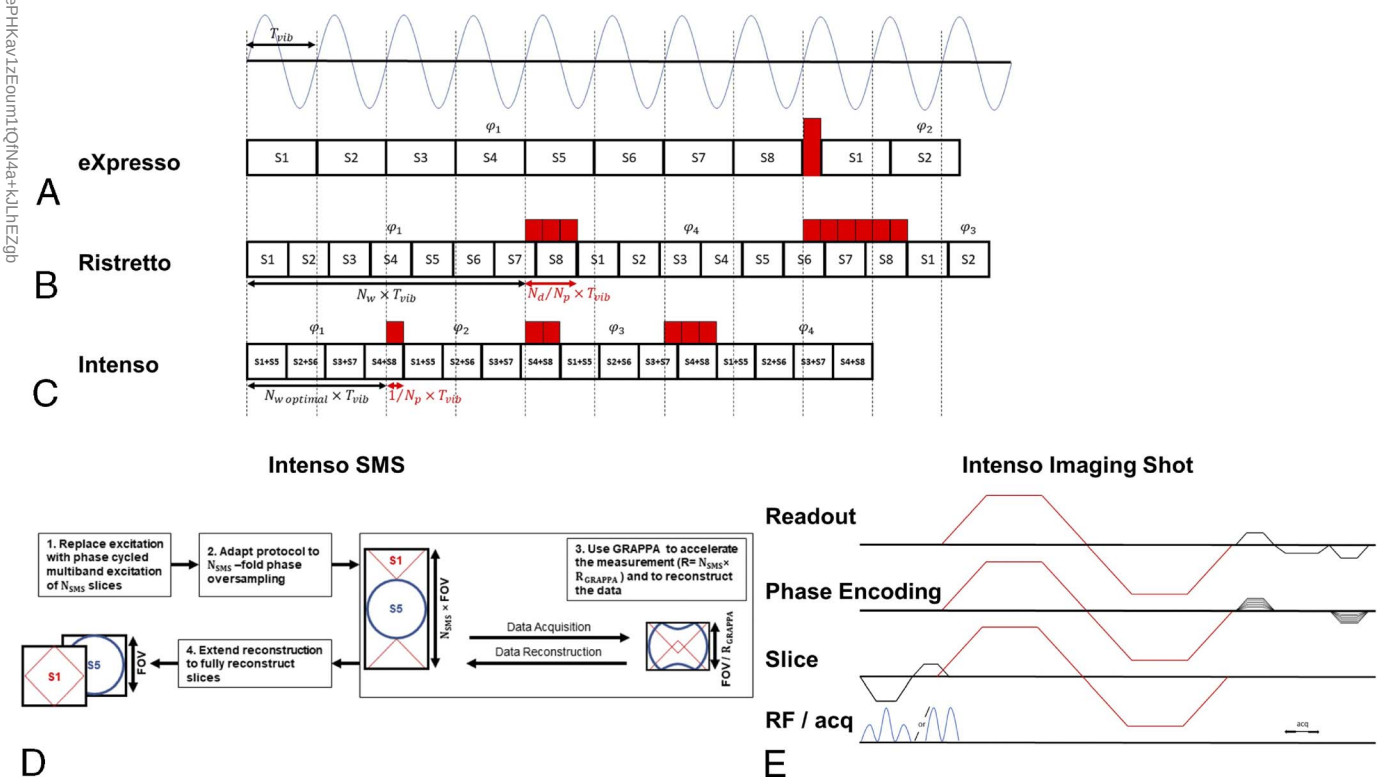

FIGURE 1. Comparison of the different MRE acquisitions with respect to their timing: a previously published multiple–breath-hold 3D MRE sequence eXpresso (A), a previously published multiple–breath-hold 3D MRE sequence Ristretto (B), and the proposed single breath-hold 3D MRE sequence Intenso (C), where each square depicts a fractional GRE-MRE imaging shot acquiring 1 (single-band excitation) or 2 (SMS excitation) slices, respectively. The red blocks indicate time delays to shift from 1 wave offset, φ_i, to another wave offset, φ_k. In case of eXpresso, successive wave offsets are acquired, that is, $k = i + 1$. For Ristretto, the shift is determined via N_d, that is, $k = i + N_d$. The proposed single breath-hold 3D MRE sequence Intenso is using optimal conditions, that is, $N_d = 1$ and $N_w = 2$. (D) Overview of the in-plane GRAPPA SMS formulation.[14] Multiband radiofrequency (RF) excitation (1), with N_{sms} oversampling (2), standard in-plane acceleration scheme (3), and FOV-splitting for slice separation (4). In our implementation, $R = 5$, $N_{sms} = 2$, and $R_i = 2.5$. (E) The proposed single breath-hold 3D MRE sequence Intenso consists of a spoiled GRE sequence (black) with dual-band RF pulses for SMS excitation (blue) and a Hadamard scheme for motion encoding (red).

undersampling (Fig. 1D). A single GRAPPA operator is used for through and in-plane dealiasing, and simple FOV splitting is performed to separate the simultaneously acquired slices.[15] (3) Using a Hadamard motion encoding scheme[14] as shown in Figure 1E, where unique combinations of the motion encoding gradients are applied on all the gradient axes (slice, readout and phase encoding) simultaneously for 4 different motion encoding measurements to encode the 3D displacement field. The Hadamard motion encoding scheme increases the sensitivity to motion, thereby mitigating the increased g-factor signal-to-noise ratio (SNR) penalty resulting from the low number of thin slices without gap and the SMS acquisition.[16,17]

The single breath-hold 3D MRE sequence imaging parameters were as follows: 8 slices, 4 mm isotropic resolution, a 96 × 66 acquisition matrix, N_{SMS} = 2, flip angle = 25 degrees, total GRAPPA acceleration factor of 5 (including in-plane and SMS acceleration) resulting in an FOV of 386 × 264 × 32 mm^3, repetition time = 9.38 milliseconds, and echo time = 7.38 milliseconds (3 T)/6.2 milliseconds (1.5 T). The motion encoding gradients of the single breath-hold 3D MRE sequence followed a Hadamard motion encoding scheme[14] and had a duration of 6.86 milliseconds (3 T)/5.68 milliseconds (1.5 T), an amplitude of 20 mT/m, and an encoding efficiency of 18.5 rad/mm (3 T) and 12.8 rad/mm (1.5 T). The final total acquisition time was 17 seconds, which could be performed in a single breath-hold by the controls and the participants.

The controls were also scanned with a previously published multiple–breath-hold 3D MRE sequence[5] for comparison. The imaging parameters of the multiple–breath-hold 3D MRE sequence were as follows: 8 slices, 4 mm isotropic resolution, a 96 × 66 acquisition matrix, flip angle = 25 degrees, in-plane GRAPPA acceleration factor of 2 resulting in an FOV of 386 × 264 × 32 mm^3, repetition time = 16.67 milliseconds, and echo time = 7.38 milliseconds (3 T). The motion encoding gradients of the multiple–breath-hold 3D MRE sequence followed an unbalanced 4-point motion encoding scheme[14] and had a duration of 6.5 milliseconds, an amplitude of 20 mT/m, and an encoding efficiency of 17.7 rad/mm. The final acquisition time was 84 seconds preformed in 4 breath-holds of 21 seconds each. In addition, 6 of the 10 controls were taken out of the scanner then completed a second MRE examination to assess the repeatability of the single breath-hold 3D MRE sequence.[18]

MRE Processing

All image processing was performed by a blinded operator with 5 years of MRE experience. Hadamard decoding was performed for each coil channel before coil combination. Afterward, the MRE phase images were unwrapped using a method based on minimum cost flow analysis.[19] Next, pixel-wise temporal Fourier transformation of the data was carried out to extract the 3D displacement field, which was then filtered using a 3D Gaussian filter of width σ = 1 pixel with 3×3 × 3 pixels support. Subsequently, all viscoelastic parameters were reconstructed by applying the curl-operator method[20] and solving for the complex k vector of the wave propagation.[2] The viscoelastic maps were calculated by averaging the 4 innermost slices, and the reported mean values of |G*|, Cs, and G" in the liver were estimated from regions of interest defined away from large vessels and organ edges using Kir software[20] (v2021, King's College London). The aforementioned MRE image processing pipeline required 120 seconds per 3D MRE dataset to generate the required viscoelastic maps. Furthermore, generic power and linear regression models were fitted to the viscoelastic parameters to establish functional dependency on the Ishak scores[2] and on the hepatic fat fraction (see Text, Supplemental Digital Content, http://links.lww.com/RLI/A799, which shows the power and linear regression models of |G*|, Cs, and G" as functions of Ishak fibrosis score, Ishak inflammation grade, and hepatic fat fraction). Finally, SNR was estimated for single and multiple–breath-hold 3D MRE sequences in the controls (see Text, Supplemental Digital Content, http://links.lww.com/RLI/A799, which estimates the SNR decrease in the single breath-hold 3D MRE sequence).

Data Statistical Analysis

To evaluate the repeatability of the single breath-hold 3D MRE sequence and its agreement with the multiple–breath-hold 3D MRE sequence in controls, the Bland-Altman method was used to study mean differences and 95% limits of agreement. The repeatability was further assessed using the intraclass correlation coefficient (ICC). Intraclass correlation coefficients and 95% confident intervals were calculated based on a 2-way mixed effects model. To assess the correlation of the viscoelastic parameters (Cs, and G") with the Ishak scores of the participants, Spearman rank correlation coefficient (ρ) and its P value were used to measure the strength of association.

All statistical analyses were performed using MATLAB software (version R2021b, Mathworks).

RESULTS

All 20 subjects underwent successful MR imaging. Of the 10 controls (group 1), 5 were female, and the mean age and BMI were 33.1 ± 9.5 years and 23.0 ± 2.1 kg/m^2, respectively. For the 10 participants (group 2), 8 were female, the mean age was 45.1 ± 16.5 years, and the mean BMI was 33.1 ± 4.0 kg/m^2, which falls within the obese range. All participants were suspected of having NAFLD, and their mean hepatic fat fraction was 12.6% ± 7.1% (Table 1).

The mean values of the measurements of |G*|, Cs, and G" in the liver of the controls (n = 10) were 1.85 ± 0.30 kPa, 1.39 ± 0.11 m/s, and 0.69 ± 0.10 kPa (G"), respectively, for the single breath-hold 3D MRE sequence and 1.81 ± 0.28 kPa, 1.38 ± 0.11 m/s, and 0.75 ± 0.14 kPa, respectively, for the multiple–breath-hold 3D MRE sequence. Bland-Altman

TABLE 1. Demographics of Patients With Nonalcoholic Fatty Liver Disease

	Mean ± SD or Median (25th–75th Percentile)
Demographic information	
Age, y	45.1 ± 16.5
BMI, kg/m^2	33.1 ± 4.0
Blood chemistry (normal range)	
Alkaline phosphatase (40–150), U/L	62 ± 16
Alanine aminotransferase (<55), U/L	56 ± 82
Aspartate aminotransferase (5–34), U/L	38 ± 38
γ-Glutamyl transferase (F 9–36 and M 12–64), U/L	59 ± 46
Bilirubin, total (0.2–1.2), mg/dL	0.99 ± 0.65
Bilirubin, direct (<0.5), mg/dL	0.38 ± 0.20
Albumin (3.5–5.2), g/dL	4.0 ± 0.3
Cholesterol (<200), mg/dL	177 ± 44
Triglycerides (<150), mg/dL	211 ± 189
HDL cholesterol (≥60), mg/dL	37 ± 10
LDL cholesterol (<100), mg/dL	103 ± 32
Glucose (70–99), mg/dL	119 ± 46
MR findings	
Magnitude of the complex-valued shear modulus, kPa	3.10 ± 1.38
Shear wave speed, m/s	1.79 ± 0.41
Loss modulus, kPa	1.14 ± 0.25
Hepatic fat fraction, %	12.6 ± 7.1
Histology (lower limit–upper limit)	
Ishak inflammation (0–18)	3 (2–8)
Ishak fibrosis (0–6)	2 (0–3)

BMI indicates body mass index; HDL, high-density lipoprotein; LDL, low-density lipoprotein; MR, magnetic resonance.

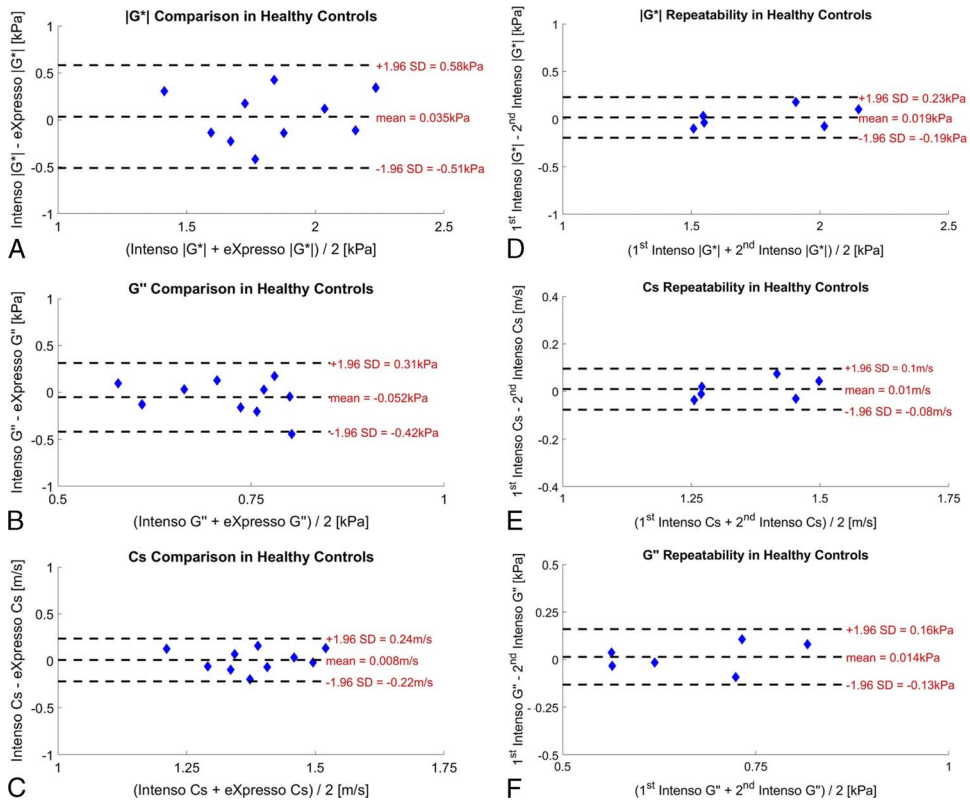

FIGURE 2. Bland-Altman plots for the comparison of the proposed single breath-hold 3D MRE sequence (Intenso) with the multiple–breath-hold 3D MRE sequence (eXpresso) for the derived viscoelastic parameters (A–C), and repeatability analysis of the single breath-hold 3D MRE sequence (Intenso) (D–F).

plots of the agreement between the single breath-hold 3D MRE sequence and the multiple–breath-hold 3D MRE sequence for the measurement of |G*|, Cs and G" in the controls (n = 10) are shown in Figures 2A–C. Bland-Altman analysis shows mean differences of 0.035 kPa for |G*| (95% limits of agreement: −0.51, 0.58), 0.008 m/s for Cs (95% limits of agreement: −0.22, 0.24), and −0.052 kPa for G" (95% limits of agreement: −0.42, 0.31), suggesting good agreement between the 2 sequences. The SNR analysis (see Text, Supplemental Digital Content, http://links.lww.com/RLI/A799, which estimates the SNR decrease in the single breath-hold 3D MRE sequence) showed a 2.3-fold decrease in the SNR of the single breath-hold 3D MRE sequence in comparison with the multiple–breath-hold 3D MRE sequence (mean relative SNR, 0.43 ± 0.07), and this decrease was statistically significant ($t_{18} = 3.76$, $P = 0.001$).

Bland-Altman analysis of the repeatability of |G*|, Cs, and G" in the controls (n = 6) using the single breath-hold 3D MRE sequence (Figs. 2D–F) shows mean differences of 0.019 kPa for |G*| (95% limits of agreement: −0.19, 0.23), 0.01 m/s for Cs (95% limits of agreement: −0.08, 0.1), and 0.014 kPa for G" (95% limits of agreement: −0.13, 0.16). The ICCs were 0.94 (95% confidence interval, 0.63–0.99) for |G*|, 0.93 (95% confidence interval, 0.61–0.99) for Cs, and 0.79 (95% confidence interval, 0.08–0.97) for G". The Bland-Altman analysis and the ICCs indicate good repeatability of the single breath-hold 3D MRE sequence.

The MRE images obtained from a representative control using the multiple–breath-hold 3D MRE sequence and the single breath-hold 3D MRE sequence are shown in Figure 3. Visual comparison of the MRE images reflects a good agreement between the 2 sequences.

Power regression models were used to report the functional dependency of Cs and G" on Ishak fibrosis score and Ishak inflammation grade, respectively, as power regression models are inclusive of linear models. In addition, no relationship was found between any of the viscoelastic parameters |G*|, Cs, G", and hepatic fat fraction (see Text, Supplemental Digital Content, http://links.lww.com/RLI/A799, which shows the power and linear regression models of |G*|, Cs, and G" as functions of Ishak fibrosis score, Ishak inflammation grade, and hepatic fat fraction).

A clear differentiation between the different Ishak fibrosis scores in the participants is visible using Cs (Fig. 4A), in particular for the challenging lower scores of fibrosis, that is, scores 0 and 1. Fitting a generic power-law model to Cs shows that its functional dependence on fibrosis is almost linear, that is, $Cs(F) \propto F^{\delta}$, with $\delta = 0.87 \pm 0.11$ ($R^2 = 0.96, P < 0.001$). The association of Cs with Ishak fibrosis score is statistically significant, with a Spearman rank correlation coefficient (ρ) of 0.95 ($P < 0.001$).

We also note that G" increases with the Ishak inflammation grades (Fig. 4B). Fitting a generic power-law to G" shows that its functional dependency on inflammation is nonlinear, that is, $G''(I) \propto I^{\delta}$, with $\delta = 0.20 \pm 0.07$ ($R^2 = 0.96$, $P < 0.001$). The correlation between G" and Ishak inflammation grade is statistically significant, with a Spearman rank correlation coefficient (ρ) of 0.84 ($P = 0.002$).

The MRE results obtained from a participant with advanced fibrosis and intermediate inflammation are shown in Figure 5. Histopathology yielded an Ishak fibrosis score of 6 and an inflammation grade of 3. Efficient penetration of the mechanical waves at 60 Hz within the liver can be observed. Elevated values for |G*| and Cs (6.38 ± 0.41 kPa and 2.57 ± 0.08 m/s, respectively) in comparison with the mean values of |G*| and Cs in the controls (1.85 ± 0.30 kPa and 1.39 ± 0.11 m/s, respectively) indicate advanced fibrosis ($P < 0.001$). Elevated G" (1.20 ± 0.3 kPa) in comparison with the mean value in controls (0.69 ± 0.10 kPa) represents inflammation ($P = 0.006$).

DISCUSSION

We evaluated the feasibility of single breath-hold 3D MRE to simultaneously quantify fibrosis and inflammation in obese patients with

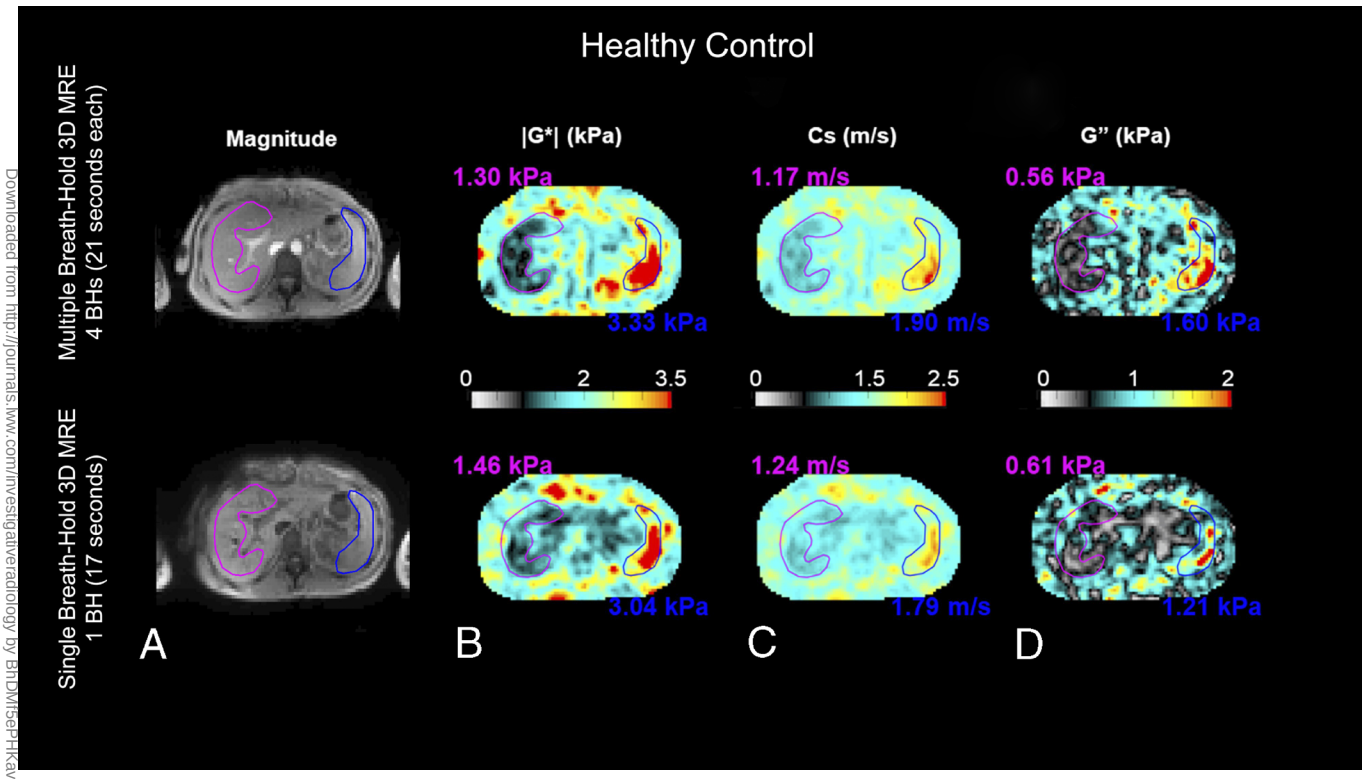

FIGURE 3. MRE for a representative control using a multiple–breath-hold 3D MRE sequence (top row) and the single breath-hold 3D MRE sequence (bottom row). The outlines of the liver and spleen are highlighted in purple and blue, respectively. (A) Magnitude images, (B) the magnitude of the complex shear modulus |G*| (kPa), (C) the shear wave speed Cs (m/s), and (D) the loss modulus G" (kPa). All maps show average values over the 4 innermost slices. The magnitude image of the multiple–breath-hold 3D MRE sequence (top row) is the magnitude of the fourth acquisition step where no motion encoding gradients are applied. On the other hand, the magnitude image of the single breath-hold 3D MRE sequence (bottom row) is the average of the magnitude images of the 4 motion encoding steps as the Hadamard motion encoding scheme applies motion encoding gradients during all 4 acquisition steps. However, visual inspection of the magnitude images shows very similar anatomical features in both sequences. Mean values of |G*|, Cs, and G" in the liver were 1.30 ± 0.35 kPa, 1.17 ± 0.15 m/s, and 0.56 ± 0.24 kPa, respectively, for the multiple–breath-hold 3D MRE sequence and 1.46 ± 0.52 kPa, 1.24 ± 0.2 m/s, and 0.61 ± 0.35 kPa, respectively, for the single breath-hold 3D MRE sequence, reflecting a good agreement between the 2 sequences.

NAFLD. The single breath-hold 3D MRE sequence provided shear wave speed and loss modulus values that correlated significantly with the Ishak fibrosis scores ($\rho = 0.95$, $P < 0.001$) and the Ishak inflammation grades ($\rho = 0.84$, $P = 0.002$), respectively. We also compared the single breath-hold 3D MRE sequence with a multiple–breath-hold 3D MRE sequence[5] in controls (n = 10), showing good agreement between the 2 methods and demonstrating high repeatability in a subset of the controls (n = 6).

The current clinical standard for MRE is a single breath-hold 2D sequence that quantifies fibrosis using the magnitude of the complex shear modulus.[21] We proposed a single breath-hold 3D MRE sequence that has the advantage of quantifying inflammation in addition to fibrosis while 2D MRE cannot differentiate between fibrosis and inflammation.[4] Inflammation accompanies fibrosis in most chronic liver disease cases; however, unlike fibrosis, the inflammatory process is not as difficult to reverse and hence early detection impacts patient management.[22,23] As a proof of concept, this single breath-hold 3D MRE sequence was evaluated in a relatively low number of participants (n = 10); however, they had a high BMI within the obese range (33.1 ± 4.0 kg/m^2). Furthermore, the proposed sequence uses an echo time that does not match an in-phase condition, which leads to signal loss because of chemical shift–induced cancellation but still provided good viscoelastic maps in participants with a high hepatic fat fraction (12.6% ± 7.1%).

We achieved a 17-second breath-hold through sequence timing optimization[6] and in-plane GRAPPA-based SMS acquisition.[15] Our experiments on the controls showed that although the SMS excitation leads to a g-factor SNR penalty,[16,17] the expected decrease in the phase-to-noise ratio of the single breath-hold 3D MRE sequence in comparison with the multiple–breath-hold 3D MRE sequence[5] was compensated by the inherent averaging of the Hadamard motion encoding scheme[14] (see Text, Supplemental Digital Content, http://links.lww.com/RLI/A799, which estimates the SNR decrease in the single breath-hold 3D MRE sequence). The expected phase-to-noise ratio penalty did not affect the image quality and thereby maintained a statistically significant correlation with biopsy grades of fibrosis and inflammation in obese patients where fatty infiltration traditionally hampers image quality. It is worth noting that the multiple–breath-hold 3D MRE sequence can also benefit from using the Hadamard motion encoding scheme to increase its sensitivity to motion in comparison with the unbalanced 4-point motion encoding scheme that is currently implemented in the multiple–breath-hold 3D MRE sequence.[14]

Simultaneous multislice excitation has been previously proposed to accelerate MRE sequences.[9] However, the 2-dimensional MRE approach proposed in Majeed et al[9] acquired 1 component of the 3D displacement field in 4 slices in a 17-second breath-hold; in comparison, the proposed sequence acquired the entire 3D displacement field in 8 slices in a single breath-hold of 17 seconds. The acquisition of the entire 3D displacement field allows for a more precise solution of the complex shear modulus because of the complex nature of the wave propagation. An accurate solution of the complex shear modulus may allow for, in addition

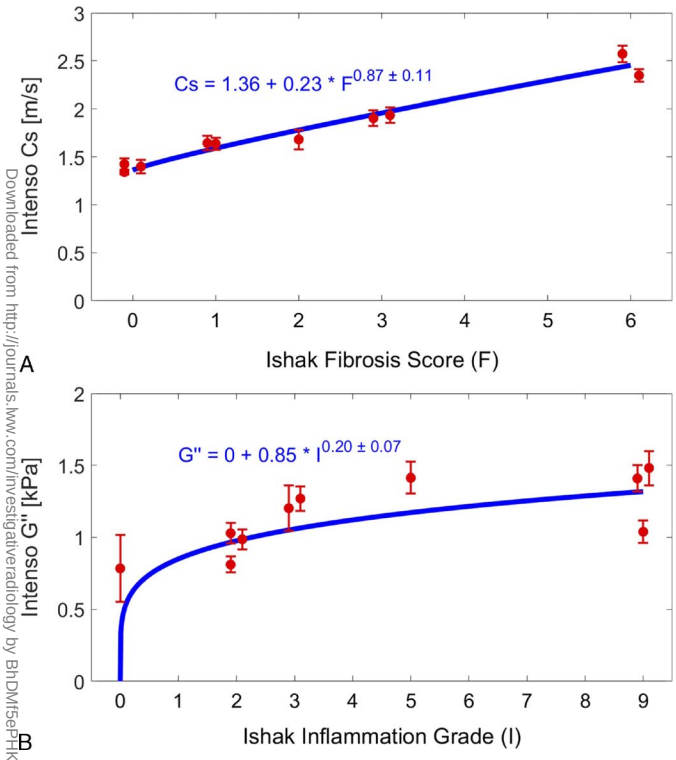

FIGURE 4. Dependence of the viscoelastic parameters measured with the single breath-hold 3D MRE sequence (Intenso) on the Ishak scores of the participants. (A) Dependence of the shear wave speed Cs (m/s) on Ishak liver fibrosis score. (B) Dependence of the loss modulus G" (kPa) on Ishak liver inflammation grade.

to fibrosis quantification, a better quantification of inflammation than the approximate solution of 2-dimensional MRE.[2–4] Moreover, free-breathing MRE techniques using either a motion-robust radial trajectory,[24] or respiratory triggering based on bellows,[25] or navigator echoes[26] have been proposed. However, these techniques lead to prolonged acquisition times for 2-dimensional MRE measurements, and their extension to acquire the full 3D displacement field would result in a considerably long acquisition time. Respiratory triggering is also known to be sensitive to drifts and variations in the breathing pattern, which may lead to blurring and ghosting artifacts.[27] Furthermore, spin-echo echo-planar imaging (EPI) sequences have been proposed for MRE and have been shown to be more robust to signal decay due to iron overload in the liver in comparison with GRE MRE sequences.[28–30] Nevertheless, spin-echo EPI MRE sequences suffer from geometrical distortions owing to the long EPI readout[31] and require optimal fat suppression to avoid off-resonance artifacts,[28] whereas the sequence proposed in this study alleviates T2*-related signal decay by using a relatively short echo time for a GRE MRE sequence.

Simultaneous assessment of liver fibrosis and inflammation using multiple–breath-hold 3D MRE has been previously investigated through either a combination of the damping ratio with the magnitude of the complex shear modulus (|G*|) at a single[3] or multiple[4] mechanical excitation frequencies or through Cs and G".[2] Multiple breath-holds lengthen the total acquisition time and might be acquired in different respiratory positions, leading to geometric misalignment and, in turn, inaccurate spatial derivatives in the reconstruction of the viscoelastic parameters. Our single breath-hold technique provided a power-law fitting of Cs and G" to their functional dependencies on fibrosis and inflammation that agrees with the results obtained in previous 3D MRE studies.[2]

A limitation of this study is that the control group consisted only of healthy volunteers with an average BMI that does not fall within the obese range (23.0 ± 2.1 kg/m^2). Ideally, obese patients with nonchronic liver disease should have served as controls. In addition, experiments in

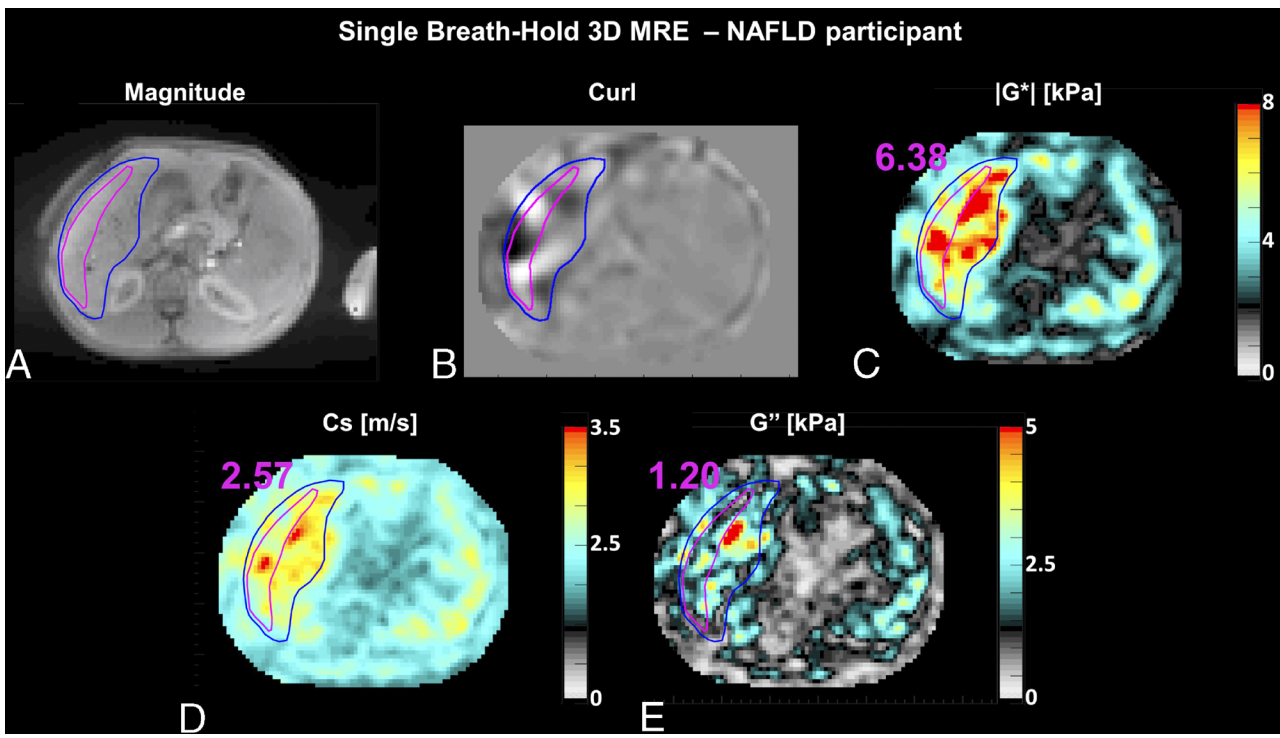

FIGURE 5. Single breath-hold 3D MRE (Intenso) for a patient with advanced fibrosis and intermediate inflammation: (A) magnitude image, (B) wave image (curl), demonstrating efficient wave penetration within the liver, (C, D, E) reconstructed images of |G*|, Cs, and G". All viscoelastic maps are averaged in the 4 innermost slices and the reported mean values are measured in the magenta-colored ROI to avoid large vessels and liver edges.

controls were evaluated only on a 3 T system but should have also been evaluated on a 1.5 T system. Moreover, the study could have included phantom experiments to validate the measured viscoelastic values.[32] Another limitation of this study is the relatively small number of patients with NAFLD. However, the study was intended as a technical development study in healthy volunteers and proof of concept in a limited number of patients with NAFLD. Furthermore, all patients with NAFLD had liver biopsies that correlated significantly with the MRE viscoelastic parameters, namely, Cs and G". The study demonstrated potential clinical application even in patients with NAFLD who are difficult to assess because of high BMI and fatty liver infiltration. Certainly, a larger clinical study is warranted to evaluate diagnostic accuracy and performance. Furthermore, the 17-second breath-hold of the proposed sequence can be long for chronic liver disease patients in the clinic, although all patients with NAFLD in this study tolerated it. Thus, further acceleration might be required to achieve a shorter breath-hold duration. The potential for the single breath-hold 3D MRE sequence in multifrequency MRE of the abdomen[33,34] and its application to other organs[35,36] are of high interest and will be addressed in future work. The single breath-hold 3D MRE sequence may benefit from the mechanical wave penetration provided by the multidriver transducer[37] currently used in multifrequency MRE to generate higher quality viscoelastic maps in the abdomen.

In conclusion, the single breath-hold 3D MRE sequence is technically feasible. It has the potential clinical value to simultaneously detect liver fibrosis and inflammation in obese patients with NAFLD. The proposed technique paves the way for the deployment of 3D MRE in the clinic since obese patients can better tolerate a single breath-hold of 17 seconds.

REFERENCES

1. Singh S, Venkatesh SK, Wang Z, et al. Diagnostic performance of magnetic resonance elastography in staging liver fibrosis: a systematic review and meta-analysis of individual participant data. *Clin Gastroenterol Hepatol*. 2015;13:440–51.e6.
2. Sinkus R, Lambert S, Abd-Elmoniem KZ, et al. Rheological determinants for simultaneous staging of hepatic fibrosis and inflammation in patients with chronic liver disease. *NMR Biomed*. 2018;31:e3956.
3. Shi Y, Qi YF, Lan GY, et al. Three-dimensional MR elastography depicts liver inflammation, fibrosis, and portal hypertension in chronic hepatitis B or C. *Radiology*. 2021;301:154–162.
4. Allen AM, Shah VH, Therneau TM, et al. The role of three-dimensional magnetic resonance elastography in the diagnosis of nonalcoholic steatohepatitis in obese patients undergoing bariatric surgery. *Hepatology*. 2020;71:510–521.
5. Garteiser P, Sahebjavaher RS, Ter Beek LC, et al. Rapid acquisition of multifrequency, multislice and multidirectional MR elastography data with a fractionally encoded gradient echo sequence. *NMR Biomed*. 2013;26:1326–1335.
6. Guenthner C, Sethi S, Troelstra M, et al. Ristretto MRE: a generalized multi-shot GRE-MRE sequence. *NMR Biomed*. 2019;32:e4049.
7. Rump J, Klatt D, Braun J, et al. Fractional encoding of harmonic motions in MR elastography. *Magn Reson Med*. 2007;57:388–395.
8. Chamarthi SK, Raterman B, Mazumder R, et al. Rapid acquisition technique for MR elastography of the liver. *Magn Reson Imaging*. 2014;32:679–683.
9. Majeed W, Kalra P, Kolipaka A. Simultaneous multislice rapid magnetic resonance elastography of the liver. *NMR Biomed*. 2020;33:e4252.
10. Lazarus JV, Colombo M, Cortez-Pinto H, et al. NAFLD—sounding the alarm on a silent epidemic. *Nat Rev Gastroenterol Hepatol*. 2020;17:377–379.
11. Ishak K, Baptista A, Bianchi L, et al. Histological grading and staging of chronic hepatitis. *J Hepatol*. 1995;22:696–699.
12. Pineda N, Sharma P, Xu Q, et al. Measurement of hepatic lipid: high-speed T2-corrected multiecho acquisition at 1H MR spectroscopy—a rapid and accurate technique. *Radiology*. 2009;252:568–576.
13. Runge JH, Hoelzl SH, Sudakova J, et al. A novel magnetic resonance elastography transducer concept based on a rotational eccentric mass: preliminary experiences with the gravitational transducer. *Phys Med Biol*. 2019;64:045007.
14. Guenthner C, Runge JH, Sinkus R, et al. Analysis and improvement of motion encoding in magnetic resonance elastography. *NMR Biomed*. 2018;31:e3908.
15. Stäb D, Speier P. Gradient-controlled local Larmor adjustment (GC-LOLA) for simultaneous multislice bSSFP imaging with improved banding behavior. *Magn Reson Med*. 2019;81:129–139.
16. Griswold MA, Jakob PM, Heidemann RM, et al. Generalized autocalibrating partially parallel acquisitions (GRAPPA). *Magn Reson Med*. 2002;47:1202–1210.
17. Barth M, Breuer F, Koopmans PJ, et al. Simultaneous multislice (SMS) imaging techniques. *Magn Reson Med*. 2016;75:63–81.
18. Manduca A, Bayly PJ, Ehman RL, et al. MR elastography: principles, guidelines, and terminology. *Magn Reson Med*. 2021;85:2377–2390.
19. Costantini M. A novel phase unwrapping method based on network programming. *IEEE Trans Geosci Remote Sensing*. 1998;36:813–821.
20. Sinkus R, Tanter M, Xydeas T, et al. Viscoelastic shear properties of in vivo breast lesions measured by MR elastography. *Magn Reson Imaging*. 2005;23:159–165.
21. Glaser KJ, Manduca A, Ehman RL. Review of MR elastography applications and recent developments. *J Magn Reson Imaging*. 2012;36:757–774.
22. Hernandez-Gea V, Friedman SL. Pathogenesis of liver fibrosis. *Annu Rev Pathol*. 2011;6:425–456.
23. dos Santos Ferreira D, Arora G, Gieseck RL 3rd, et al. Molecular magnetic resonance imaging of liver fibrosis and fibrogenesis is not altered by inflammation. *Invest Radiol*. 2021;56:244–251.
24. Kafali SG, Armstrong T, Shih SF, et al. Free-breathing radial magnetic resonance elastography of the liver in children at 3 T: a pilot study. *Pediatr Radiol*. 2022;52:1314–1325.
25. Wang H, Tkach JA, Trout AT, et al. Respiratory-triggered spin-echo echo-planar imaging-based MR elastography for evaluating liver stiffness. *J Magn Reson Imaging*. 2019;50:391–396.
26. Murphy IG, Graves MJ, Reid S, et al. Comparison of breath-hold, respiratory navigated and free-breathing MR elastography of the liver. *Magn Reson Imaging*. 2017;37:46–50.
27. Zaitsev M, Maclaren J, Herbst M. Motion artifacts in MRI: a complex problem with many partial solutions. *J Magn Reson Imaging*. 2015;42:887–901.
28. Choi SL, Lee ES, Ko A, et al. Technical success rates and reliability of spin-echo echo-planar imaging (SE-EPI) MR elastography in patients with chronic liver disease or liver cirrhosis. *Eur Radiol*. 2020;30:1730–1737.
29. Serai SD, Trout AT. Can MR elastography be used to measure liver stiffness in patients with iron overload? *Abdom Radiol (NY)*. 2019;44:104–109.
30. Yoon JW, Lee ES, Park HJ, et al. Comparison of spin-echo echo-planar imaging magnetic resonance elastography with gradient-recalled echo magnetic resonance elastography and their correlation with transient elastography. *Diagn Interv Radiol*. 2022;28:294–300.
31. Jezzard P, Balaban RS. Correction for geometric distortion in echo planar images from B0 field variations. *Magn Reson Med*. 1995;34:65–73.
32. Morr AS, Herthum H, Schrank F, et al. Liquid-liver phantom: mimicking the viscoelastic dispersion of human liver for ultrasound- and MRI-based elastography. *Invest Radiol*. 2022;57:502–509.
33. Hudert CA, Tzschätzsch H, Rudolph B, et al. Tomoelastography for the evaluation of pediatric nonalcoholic fatty liver disease. *Invest Radiol*. 2019;54:198–203.
34. Lin H, Wang Y, Zhou J, et al. Tomoelastography based on multifrequency MR elastography predicts liver function reserve in patients with hepatocellular carcinoma: a prospective study. *Insights Imaging*. 2022;13:95.
35. Prezzi D, Neji R, Kelly-Morland C, et al. Characterization of small renal tumors with magnetic resonance elastography: a feasibility study. *Invest Radiol*. 2018;53:344–351.
36. Asbach P, Ro S-R, Aldoj N, et al. In vivo quantification of water diffusion, stiffness, and tissue fluidity in benign prostatic hyperplasia and prostate cancer. *Invest Radiol*. 2020;55:524–530.
37. Dittmann F, Tzschätzsch H, Hirsch S, et al. Tomoelastography of the abdomen: tissue mechanical properties of the liver, spleen, kidney, and pancreas from single MR elastography scans at different hydration states. *Magn Reson Med*. 2017;78:976–983.